JACS
JOURNAL OF THE AMERICAN CHEMICAL SOCIETY
pubs.acs.org/JACS
Article

Isomer-Dependent Electron Affinities of Fluorophenyl Radicals, $^{\bullet}C_6H_{5-x}F_x$ ($2 \leq x \leq 4$)

Kristen Rose McGinnis, Conor J. McGee, and Caroline Chick Jarrold*

Cite This: J. Am. Chem. Soc. 2024, 146, 7063−7075
Read Online
ACCESS | Metrics & More | Article Recommendations | Supporting Information

ABSTRACT: Di-, tri-, and tetrafluorophenyl radicals each have three regioisomers, several of which can form multiple distinct radical structures. We present the photoelectron spectra of the di-, tri-, and tetrafluorophenide regioisomer anions generated from their associated fluorobenzene precursors. By comparing the spectra to the results of density functional theory calculations, we determine that in cases where more than one possible radical isomer is possible for a given regioisomer (radicals formed from 1,2-difluorobenzene, 1,3-difluorobenzene, 1,2,3-trifluorobenzene, and 1,2,4-trifluorobenzene) the most stable anion corresponds to a less stable neutral, suggesting that the reactive C-center on these fluorine-substituted phenyl groups can be controlled by charge state. Full analyses of the spectra and computational results yield further insights into the differences between the electronic and molecular structures of the fluorophenyl radicals and their associated anions.

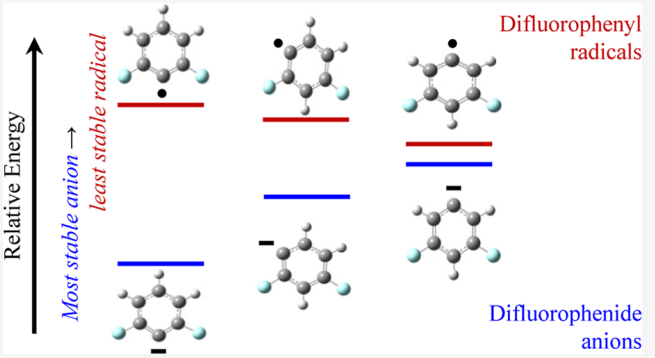

1. INTRODUCTION

The structure and reactivity of the phenyl radical have been the topics of numerous spectroscopic investigations.[1−8] The phenyl radical, formed from benzene via simple homolytic C−H bond cleavage, conserves the aromaticity of benzene but is nonetheless highly reactive. As an intermediate in combustion of aromatic hydrocarbons, polycyclic aromatic hydrocarbon formation, and soot formation,[9,10] it has implications in health and environmental concerns. The phenyl radical is also an important reactant in astrochemistry.[11−13]

The reactivity[14] and electronic structures[15] of aromatic rings are known to be strongly influenced by substituents on the ring. For example, a fluorine substituent on benzene contributes a lone pair to resonance stabilization but is highly electronegative. The inductive effect of fluorine is weakly deactivating and leaves the C−H bond opposite to the C−F bond the weakest.[16] In other words, the most stable fluorophenyl radical has the radical center opposite the C−F. There have been fewer studies on the impact of further −F substitution on the phenyl radical. From a thermodynamic standpoint, the lowest energy path to formation of fluorophenyl radicals from any fluorobenzene (with the obvious exception of hexafluorobenzene) would again involve homolytic C−H dissociation as the C−F bond is ca. 0.7 eV stronger than C−H bond.[17]

In a series of related studies on fluorine-substituted benzenes[18−20] and fluorophenyl radicals,[21] our group demonstrated how fluorination of benzene and the phenyl radical affect how strongly these molecules bind electrons[19,21] or molecular anions[18,20] using anion photoelectron (PE) spectroscopy and supporting density functional theory (DFT) calculations.[21] The fluorine-substituted phenyl radicals, $^{\bullet}C_6H_{5-x}F_x$ ($1 \leq x \leq 4$), in particular, showed a straightforward, monotonic increase in EA. This effect is readily explained: The excess charge resides in the in-plane sp^2 orbital that coincides with the radical center in the neutral. Because the C_6 ring becomes increasingly positively charged with the number of electron-withdrawing −F substituents, the "extra" electron becomes more strongly bound to the C_6 ring.

The specific regioisomers of the $C_6H_{6-x}F_x$ ($2 \leq x \leq 4$) fluorobenzene molecule precursors used to generate the radicals in the previous study[21] were those with zero dipole moments by symmetry (1,4-difluorobenzene, 1,3,5-trifluorobenzene, and 1,2,4,5-tetrafluorobenzene). The rationale behind this selection of regioisomers was the avoidance of dipoles introducing nonvalence-bound anions, which has been observed in other systems.[22] Of course, C_6H_5F does have a dipole moment, and it is also distinguished from the more

Received: January 12, 2024
Revised: February 15, 2024
Accepted: February 22, 2024
Published: March 5, 2024

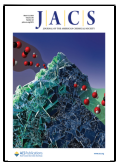

https://doi.org/10.1021/jacs.4c00556
J. Am. Chem. Soc. 2024, 146, 7063−7075

fluorinated benzenes in the series in that the $^{\bullet}C_6H_4F$ radical can assume three possible structures depending on whether the radical center is ortho, meta, or para to the fluorinated C center, which we will now simply refer to as "C−F." In contrast, the $^{\bullet}C_6H_{5-x}F_x$ ($2 \le x \le 4$) radicals, given the regioisomers of the $C_6H_{6-x}F_x$ ($2 \le x \le 4$) precursors noted above, have only one possible structure. An unanticipated computational result was that the lowest energy structure of the fluorophenide anion, in which the negative charge was localized on the $^{\bullet}$C-center ortho to the C−F, did not coincide with the most stable structure of the neutral radical, in which, as noted above, the radical center is para to the C−F.

Fluorophenyl substituents play an important role in novel antibiotic resistance and cancer therapy drugs,[23−26] in addition to improving ligand affinities compared to phenyl substituents.[27,28] These drugs have been shown to have different efficacies when the fluorine is located at different positions on the phenyl substituents.[23] While the structures of fluorophenyl radical reactants can be controlled with leaving groups at the targeted radical position relative to the C−F positions, carbanions may offer another tool in the synthetic toolbox,[29] and our results suggest the potential utility of fluorophenide anions in these syntheses.

In this report, we present the anion PE spectra of the fluorophenide anions $C_6H_{5-x}F_x^-$ ($2 \le x \le 4$) generated from all three different structural isomers of $^{\bullet}C_6H_{5-x}F_x$ ($2 \le x \le 4$) for each x. For fluorophenyl radicals that can form more than one structure, the results show strong evidence that the most stable isomers of the $C_6H_{5-x}F_x^-$ ($x = 2, 3$) anions correspond to less stable neutral radical structures. The reactive center on the most stable neutral radical is therefore different from the reactive center on the most stable anion in any case where multiple structures are possible. This finding, again, raises the possibility of a carbanion handle on structure control of fluorophenyl groups through carbanion chemistry.

Anion PE spectroscopy is a technique that is particularly well-suited for the study of neutral radicals, as is reflected in the literature.[30−50] The PE spectra of $C_6H_{5-x}F_x^-$ ($2 \le x \le 4$) presented here are similar in profile, but all show distinct electron affinities (EAs), suggesting that the position of the F-centers on the C_6 ring is preserved when the precursors undergo homolytic C−H bond dissociation and form anions. Combining the experimental and computational results, we determine that the relative energies of the neutral $^{\bullet}C_6H_{5-x}F_x$ radicals with a particular value of x fall in a fairly narrow window of energy (<0.4 eV) while the relative energies of the associated anions are more sensitive to the position of the −F substituents as well as the position of the excess charge relative to the −F substituents.

2. METHODS

2.1. Experimental Details. As descriptions of the apparatus[51] and the photoemission ion source[52] used for generating the anions of interest in this study have been published previously, we provide just a brief outline of the experimental details here. The experiments were completed using an apparatus capable of anion generation, mass selection, and photodetachment spectroscopy. To produce the fluorophenide anions, $C_6H_{5-x}F_x^-$ ($2 \le x \le 4$), precursor fluorobenzenes were heated in a high-pressure reservoir in line with an ultrahigh purity helium gas line maintained at 80 psig. The fluorobenzenes selected for this study include 1,2-difluorobenzene (Thermo Scientific, 98% purity), 1,3-difluorobenzene (Santa Cruz Biotechnology, 98% purity), 1,4-difluorobenzene (Aldrich, 99% purity), 1,2,3-trifluorobenzene (AmBeed, 98.50% purity), 1,2,4-trifluorobenzene (Santa Cruz Biotechnology, 98% purity), 1,3,5-trifluorobenzene (Sigma-Aldrich, 97% purity), 1,2,3,4-tetrafluorobenzene (AmBeed, 98% purity), 1,2,3,5-tetrafluorobenzene (AmBeed 99.60%), and 1,2,4,5-tetrafluorobenzene (Santa Cruz Biotechnology, 98% purity). The fluorobenzene/He gas mixture was introduced into the ion source by using a pulsed molecular beam valve operating at 30 Hz. The source houses a Gd_2O_3 target parallel with the direction of the expansion. The attenuated second harmonic output (1 mJ/pulse of 532 nm; $h\nu$ = 2.330 eV) of a Nd/YAG laser, also operating at 30 Hz, was timed to hit the Gd_2O_3 target while the gas was flowing over the surface. Care was taken to purge the system when switching between samples.

The resulting charged and neutral molecules were thermalized in a 10 mm long, 3 mm diameter channel before being expanded into the vacuum chamber. The expansion was collimated with a 3 mm skimmer, and the anions were then accelerated into a 0.94 m Bakker-style time-of-flight mass spectrometer. The ions passed through a mass defining slit into a detector region and collided with a dual microchannel detector assembly at the end of the drift path.

Fifteen cm upstream of the ion detector, the mass-separated anions of interest were selectively detached using a pulsed Nd/YAG laser. Both the second (532 nm, 2.330 eV) and third (355 nm, 3.495 eV) harmonic outputs were used in this study.

The PE kinetic energies are related to the photon energy ($h\nu$), the neutral EA, and the initial anion (E_{int}^{anion}) and final neutral states ($E_{int}^{neutral}$) via

$$e_{KE}^- = h\nu - EA - E_{int}^{neutral} + E_{int}^{anion} \quad (1)$$

Assuming the anions are internally cold ($E_{int}^{anion} \approx 0$), the e_{KE}^- distribution largely reflects the energy levels of the neutral that are accessed by one-electron transitions from the initial anion state. In practice, incomplete vibrational and rotational cooling does result in some congestion of spectroscopic features. In order to more easily compare spectra obtained with different photon energies, the spectra presented below are plotted as a function of electron binding energy (e_{BE}^-)

$$e_{BE}^- = h\nu - e_{KE}^- \quad (2)$$

which is independent of photon energy. The e_{BE}^- values equal the energy difference between the final neutral and initial anion states.

The photodetachment takes place at the intersection of the ion drift path and a velocity map imaging (VMI) setup.[53,54] The resulting PEs are projected onto a 70 mm dual microchannel plate/phosphor screen, and the resulting PE images were captured with a charge-coupled device(camera, with the images saved using NuACQ 0.9 developed by the Suits group.[55] The three-dimensional velocity distributions were extracted from the two-dimensional image using the BASEX program,[56] and the resulting speed distribution was converted to electron kinetic energy (e_{KE}^-) by calibration against the well-known PE spectrum of O_2^-.[57]

In addition to determining the e_{BE}^- values from the PE spectra, the images also show photoelectron angular distributions (PADs). The PADs presented below were generated by integrating plots of slices of the image cut at different angles relative to the electric field polarization of the detachment laser.

The PE images were collected from over 108,000 to 1,063,800 shots. The number of laser shots for each image is included in the Supporting Information. The resolution of the instrument is dependent on e_{KE}^-; $\frac{\Delta e_{KE}^-}{e_{KE}^-} = 0.025$.

2.2. Computational Details. The molecular structures of the intact fluorophenyl neutral and fluorophenide anions that would be formed by a single C−H bond dissociation were optimized using B3LYP/aug-cc-pVTZ, a computationally expedient approach that has yielded good agreement with experiments in previous studies.[58] The atomic polar tensor (APT) resulting directly from the computations was used to qualitatively compare charge distributions in the molecules targeted in this study. All calculations were performed using the Gaussian 16 suites for electronic structure calculations.[59]

https://doi.org/10.1021/jacs.4c00556
J. Am. Chem. Soc. 2024, 146, 7063−7075

Radicals and associated anions formed from both 1,2-difluorobenzene and 1,2,3-trifluorobenzene can form two distinct structures, and radicals and anions formed from 1,3-difluorobenzene and 1,2,4-trifluorobenzene can form three potential structures, and all were taken into account computationally. We verified that the computed structures were local minima by confirming that all vibrational frequencies were nonimaginary.

To compare the computational results more directly with the experimental anion PE spectra, the adiabatic EAs were calculated from the difference between the zero-point corrected energies of the optimized anions and neutrals. Further, the computed vertical detachment energy (VDE), which corresponds to the electron binding energy where the vibrational manifold of the detachment transition is most intense (i.e., maximum Franck−Condon overlap), was determined from the difference between the electronic energy of the neutral radical confined to the optimized structure of the anion and the electronic energy of the optimized anion.

While the experimental spectra presented below do not exhibit vibrationally resolved features, the Supporting Information includes spectral simulations based on computed structures, vibrational coordinates, vibrational frequencies, and relative energies. These simulations were generated using home-written Labview codes, which have been described in detail previously.[60]

3. RESULTS AND DISCUSSION

3.1. PE Spectra. Figures 1−3 show the anion PE spectra of the di-, tri-, and tetrafluorophenyl radicals generated from the three regioisomers of di-, tri-, and tetrafluorobenzene precursors, respectively. The blue traces are the spectra obtained using 3.495 eV photon energy, and the green traces are the spectra obtained using 2.330 eV photon energy. The raw and reconstructed images are included in the Supporting Information. We note here that within each value of x, where x indicates the number of fluorine substitutions, the order in which the spectra and computed structures are presented will be (1) all x F atoms situated on adjacent C atoms; (2) $(x-1)$ F atoms on adjacent C atoms; and (3) F atoms maximally separated. For the remainder of the manuscript, we will refer to these as group 1, group 2, and group 3, respectively.

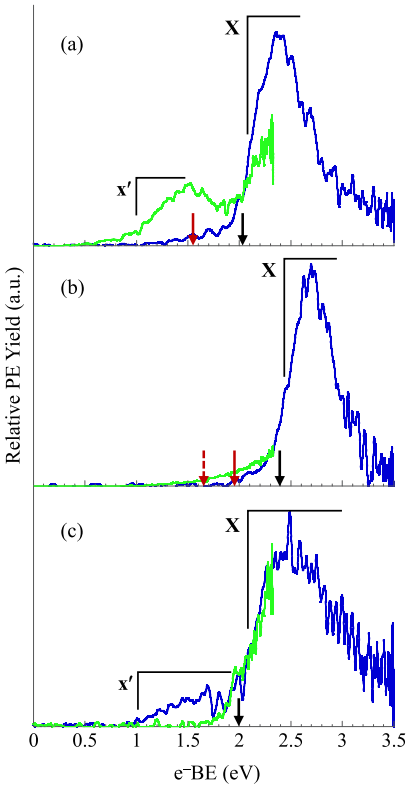

Figure 1. Anion PE spectra of the difluorophenide anions generated from (a) 1,2-difluorobenzene, (b) 1,3-difluorobenzene, and (c) 1,4-difluorobenzene obtained using 3.495 eV (blue traces) and 2.33 eV (green traces). Band energies are summarized in Table 1. The black and red arrows pointing to the e_{BE}^- axis indicate computed adiabatic EAs (see text in Section 3.1). Panel (c) adapted with permission from ref 21. Copyright 2023 American Chemical Society.

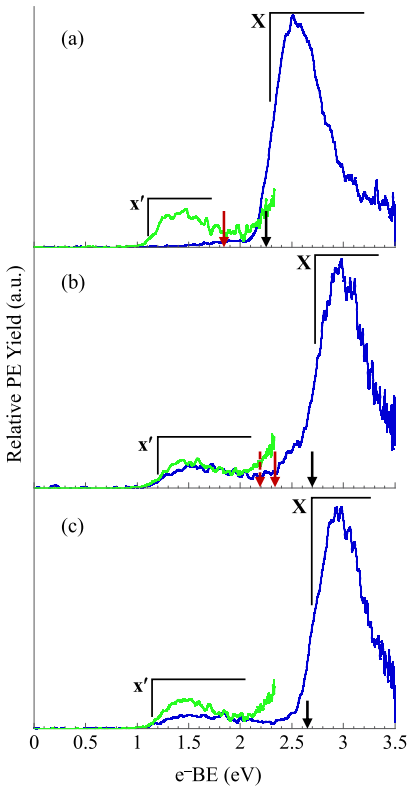

Figure 2. Anion PE spectra of the trifluorophenide anions generated from (a) 1,2,3-trifluorobenzene, (b) 1,2,4-trifluorobenzene, and (c) 1,3,5-trifluorobenzene obtained using 3.495 eV (blue traces) and 2.33 eV (green traces). Band energies are summarized in Table 2. The black and red arrows pointing to the e_{BE}^- axis indicate computed adiabatic EAs (see text in Section 3.1). Panel (c) adapted with permission from ref 21. Copyright 2023 American Chemical Society.

Plots of the PADs determined for each spectrum are shown in Figure 4. In direct photodetachment of randomly oriented anions with a linearly polarized laser, Zare developed the expression to describe the PADs[61]

$$\frac{d\sigma}{d\Omega} = \frac{\sigma}{4\pi}\left[1 + \frac{\beta}{2}(3\cos^2\theta - 1)\right] \quad (3)$$

In this expression, σ is the total photodetachment cross section, $\frac{d\sigma}{d\Omega}$ is the differential cross section with respect to the solid angle ($d\Omega = \sin\theta\, d\theta$), θ is the angle between the ejected electrons and the electric field vector of the laser, and β is an e_{KE}^--dependent anisotropy parameter that can have values between −1 and 2. The value of β is governed by conservation of angular momentum.[62,63] For example, in atomic systems, detachment from s-orbitals ($l = 0$) results in PEs with $l = 1$ (p-wave), which would have $\beta = 2$, or parallel ($\cos^2\theta$) PADs. The β values determined for each spectrum using the expression

https://doi.org/10.1021/jacs.4c00556
J. Am. Chem. Soc. 2024, 146, 7063−7075

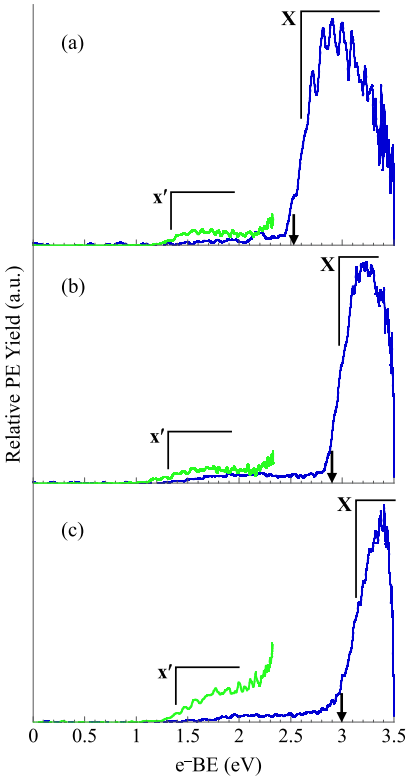

Figure 3. Anion PE spectra of the tetrafluorophenide anions generated from (a) 1,2,3,4-tetrafluorobenzene, (b) 1,2,3,5-tetrafluorobenzene, and (c) 1,2,4,5-tetrafluorobenzene obtained using 3.495 eV (blue traces) and 2.33 eV (green traces). Band energies are summarized in Table 3. The black and red arrows pointing to the e_{BE}^- axis indicate computed adiabatic EAs (see text in Section 3.1). Panel (c) adapted with permission from ref 21. Copyright 2023 American Chemical Society.

$$\beta = \frac{I_{\parallel} - I_{\perp}}{\frac{1}{2}I_{\parallel} + I_{\perp}} \tag{4}$$

are included in Figure 4. The dotted lines shown in Figure 4b,c are the fits of the PADs with the poorest signal-to-noise ratio to confirm the validity of the β values determined using eq 4.

Mass spectra of anions generated from all nine precursors are also included in the Supporting Information and show that no anions of the intact fluorobenzene precursors are formed in the ion source. Only the fluorophenide anions and other molecular fragment anions are observed. The spectra will now be described in more detail.

3.1.1. Difluorophenides. Figure 1 shows the PE spectra of the anions formed from (a) 1,2-difluorobenzene, (b) 1,3-difluorobenzene, and (c) 1,4-difluorobenzene, the latter of which was published previously[21] but included here for direct comparison. The black and red arrows pointing to the e_{BE}^- axes indicate computed adiabatic EAs, which are described below.

The three spectra are qualitatively similar in appearance, each showing an intense, vibrationally broadened feature, **X**, in the 2.0−3.0 eV window of energy. Two spectra also exhibit distinct signal tailing to lower e_{BE}^- values, labeled **x**′, which, as discussed in a previous study, changes in intensity with deterioration of the gadolinia photoemitter and may be due to a fulvenide or other structural isomer of the anion.[21]

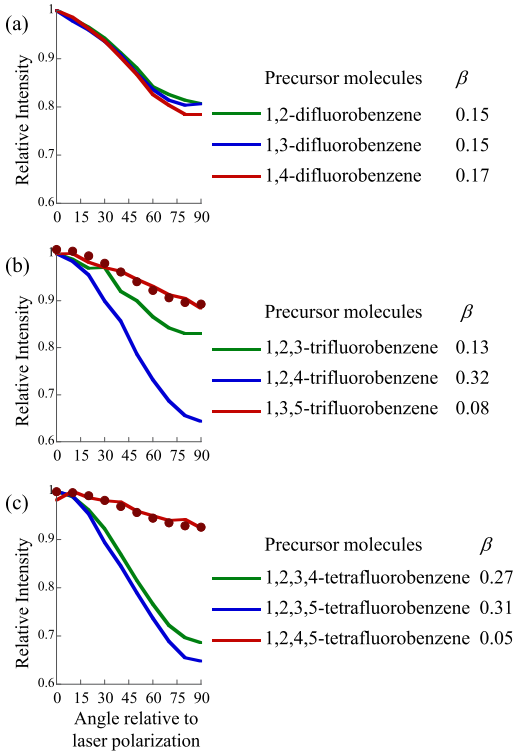

Figure 4. Plots of the relative intensities of bands X with respect to the angle relative to the laser polarization, or PADs, in the spectra of the (a) difluorophenide anions (Figure 1), (b) trifluorophenide anions (Figure 2), and (c) tetrafluorophenides (Figure 3). Raw and reconstructed PE images from which the plots were generated are included in the Supporting Information. The green traces correspond to precursor $C_6H_{6-x}F_x$ structures having all F atoms on adjacent C atoms (group 1), blue traces correspond to precursor fluorobenzene structures in which $x - 1$ F atoms are on adjacent C atoms (group 2), and red traces correspond to maximally separated F atoms (group 3). The solid red circles in (b,c) follow the curve generated by substituting the β values for the associated spectra (e.g., 0.08 and 0.05, respectively) into eq 3.

Despite the qualitative similarities, bands **X** exhibit different bandwidths and appear at different energies for the anions generated from the three precursor regioisomers. Determining the origin of broad transitions that do not exhibit resolved vibrational features is inherently difficult, but for the sake of consistency, we have selected the first distinct shoulder on the rising e⁻BE edge of band **X** as the origin, based on the general similarities between the phenide[8] and fluorophenide[21] spectral profiles. This energy also coincides with the position at which the low-e_{BE}^- rising edge reaches approximately half of the maximum intensity. Based on these origins, the EAs of the $^{\bullet}C_6H_3F_2$ radicals generated from 1,2-difluorobenzene, 1,3-difluorobenzene, and 1,4-difluorobenzene are 2.11 ± 0.10, 2.45 eV ± 0.10, and 2.07 ± 0.15 eV, respectively. The uncertainty is conservative, more so for the radical formed from 1,4-difluorbenzene. The anion was formed only when higher laser powers were used in the ion source, which likely resulted in more vibrationally excited anions compared to the others. The EAs and VDEs determined from each spectrum are summarized in Table 1.

3.1.2. Trifluorophenides. Figure 2 shows the PE spectra of the anions formed from (a) 1,2,3-trifluorobenzene, (b) 1,2,4-trifluorobenzene, and (c) 1,3,5-trifluorobenzene, the latter of which was published previously[21] but again included here for

https://doi.org/10.1021/jacs.4c00556
J. Am. Chem. Soc. 2024, 146, 7063−7075

Table 1. Summary of Computed Zero-Point Corrected Energies Relative to the 2,6-Difluorophenide Anion (the Lowest Anion of All Difluorophenides), Shown Graphically in Figure 5, in Addition to Adiabatic Detachment Energies, and Vertical Detachment Energies, for the Anionic Difluorophenides and Corresponding Neutral Radicals[a]

molecule		electronic term	relative E (eV)	ADE/VDE (eV)	Exp ADE/VDE
1,2-difluorobenzene precursor	2,3-difluorophenyl radical	$^2A'$	2.45	2.03/2.34	2.11 ± 0.10/2.38 ± 0.05
	3,4-difluorophenyl radical	$^2A'$	2.39	1.56/2.35	
	3,4-difluorophenide	$^1A'$	0.83		
	2,3-difluorophenide	$^1A'$	0.42		
1,3-difluorophenide precursor	2,6-difluorophenyl radical	$^2A_1$	2.40	2.40/2.75	2.49 ± 0.10/2.69 ± 0.05
	2,4-difluorophenyl radical	$^2A'$	2.32	1.95/2.68	
	3,5-difluorophenyl radical	$^2A_1$	2.20	1.65/2.60	
	3,5-difluorophenide	$^1A_1$	0.55		
	2,4-difluorophenide	$^1A'$	0.37		
	2,6-difluorophenide	$^1A_1$	0.00		
1,4-difluorophenide precursor	2,5-difluorophenyl radical	$^2A'$	2.32	2.00/2.35	2.07 ± 0.15/2.48 ± 0.05
	2,5-difluorophenide	$^1A'$	0.32		

[a]Computed energies for 2,5-difluorophenyl and 2,5-difluorophenide were also reported in ref 21 and included here with permission from ref 21. Copyright 2023 American Chemical Society.

Table 2. Summary of Computed Zero-Point Corrected Energies Relative to the 2,4,6-Trifluorophenide Anion (the Lowest Anion of All Trifluorophenides), Shown Graphically in Figure 6, in Addition to Adiabatic Detachment Energies, and Vertical Detachment Energies, for the Anionic Trifluorophenides and Corresponding Neutral Radicals[a]

molecule		electronic term	relative *E* (eV)	ADE/VDE (eV)	Exp ADE/VDE
1,2,3-trifluorobenzeneprecursor	2,3,4-trifluorophenyl radical	$^2A'$	2.83	2.23/2.55	2.30 ± 0.10/2.52 ± 0.05
	3,4,5-trifluorophenyl radical	$^2A_1$	2.74	1.92/2.35	
	3,4,5-trifluorophenide	$^1A_1$	0.90		
	2,3,4-trifluorophenide	$^1A'$	0.60		
1,2,4-trifluorophenide precursor	2,3,6-trifluorophenyl radical	$^2A'$	2.78	2.70/3.03	2.71 ± 0.10/2.98 ± 0.05
	2,4,5-trifluorophenyl radical	$^2A'$	2.70	2.21/2.56	
	2,3,5-trifluorophenyl radical	$^2A'$	2.67	2.32/2.65	
	2,3,5-trifluorophenide	$^1A'$	0.35		
	2,4,5-trifluorophenide	$^1A'$	0.49		
	2,3,6-trifluorophenide	$^1A'$	0.08		
1,3,5-trifluorophenide precursor	2,4,6-trifluorophenyl radical	$^2A_1$	2.63	2.63/2.99	2.69 ± 0.10/2.98 ± 0.05
	2,4,6-trifluorophenide	$^1A_1$	0.00		

[a]Computed energies for 2,4,6-trifluorophenyl and 2,4,6-trifluorophenide were also reported in ref 21 and included here with permission from ref 21. Copyright 2023 American Chemical Society.

direct comparison. The spectra are qualitatively similar to each other as well as to the spectra of the anions generated from the difluorobenzene precursors, including the presence of the predominant, vibrationally broadened but unresolved band **X**, and the presence of the lower-intensity band **x′**, appearing at lower e_{BE}^-. Using the convention noted above, the EAs of the $^{\bullet}C_6H_2F_3$ radicals generated from 1,2,3-trifluorobenzene, 1,2,4-trifluorobenzene, and 1,3,5-trifluorobenzene are 2.30 ± 0.10, 2.71 eV ± 0.10, and 2.69 ± 0.10 eV, respectively. These values along with the VDEs are summarized in Table 2.

3.1.3. Tetrafluorophenides. Figure 3 shows the PE spectra of the anions formed from (a) 1,2,3,4-tetrafluorobenzene, (b) 1,2,3,5-tetrafluorobenzene, and (c) 1,2,4,5-tetrafluorobenzene, the latter of which was published previously[21] but again included here for direct comparison. The increase in the EAs of the neutral radicals relative to those reflected in Figures 1 and 2 is more in evidence in Figure 3b,c, as band **X** is partially truncated at the high e_{BE}^- end of the spectra. Using the convention noted above, the EAs of the $^{\bullet}C_6HF_4$ radicals generated from 1,2,3,4-tetrafluorobenzene, 1,2,3,5-tetrafluorobenzene, and 1,2,4,5-tetrafluorobenzene are 2.63 ± 0.10 eV, 2.97 eV ± 0.10 eV, and 3.11 ± 0.10 eV, respectively.

3.1.4. PADs. Figure 4 shows the plots of the PADs of the three PE spectra obtained for (a) difluorophenides, (b) trifluorophenides, and (c) tetrafluorophenides. Figure 4a shows that the PADs of all three difluorophenide structures are nearly identical, with all being modestly parallel. The values of β range from 0.15 to 0.17. In contrast, the PADs determined for the tri- and tetrafluorophenide spectra range from nearly isotropic for the maximally spaced F^- atom structures (group 3) to over 0.3.

Based on previous studies,[21,30−37,48−50] the excess electron pairs with the radical center and is localized in an in-plane sp^2 orbital, which would be consistent with a PAD that is intermediate between parallel and isotropic.[64,65] In an attempt to better understand the differences in the PADs, as well as the differences in EAs among the different structures, we consider the computational results on the structures and energies of the radicals and their associated anions.

3.2. Computational Results. *3.2.1. Relative Energies of Anions and Radicals.* Figures 5− 7 summarize the relative energies of all the radicals and associated anions that could be formed via homolytic C−H bond dissociation of the three regioisomers of di-, tri-, and tetrafluorobenzene. The results for

https://doi.org/10.1021/jacs.4c00556
J. Am. Chem. Soc. 2024, 146, 7063−7075

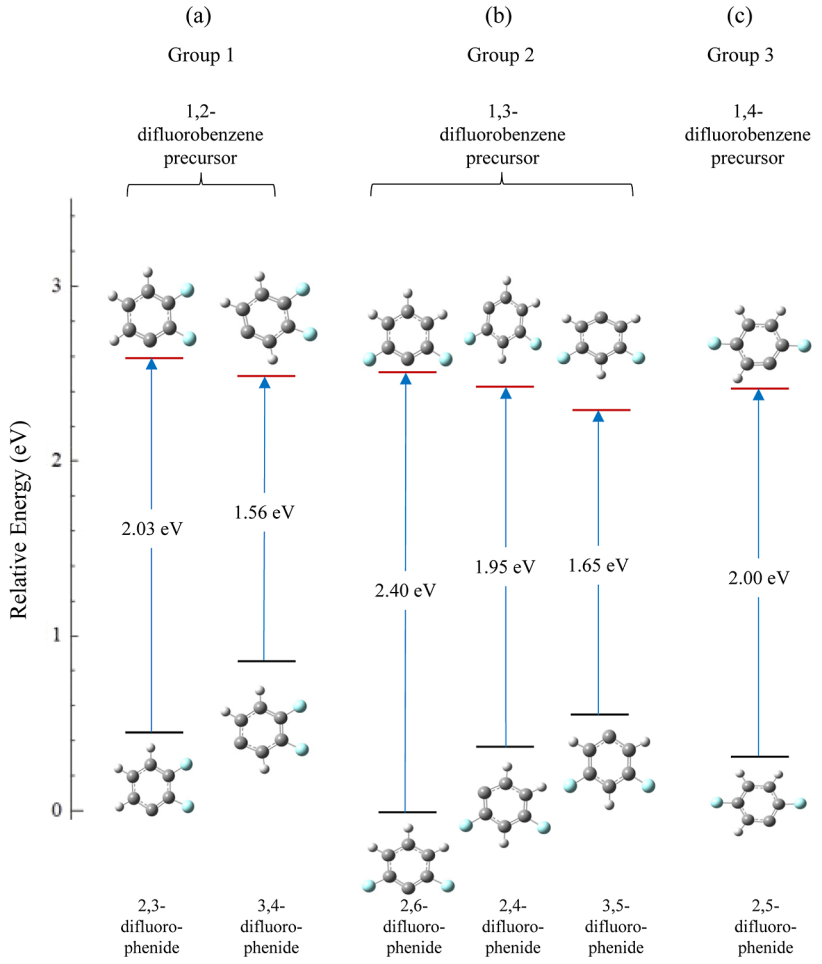

Figure 5. Computed relative energies of the neutral radicals and associated anions generated from homolytic C−H bond dissociation for (a) 1,2-difluorobenzene (group 1), (b) 1,3-difluorobenzene (group 2), and (c) 1,4-difluorobenzene (group 3). The arrows connecting the anions to the associated neutral radicals are labeled with the computed adiabatic EAs, which are additionally indicated by arrows on the experimental spectra shown in Figure 1.

the species formed from 1,4-difluorobenzene, 1,3,5-trifluorobenzene, and 1,2,4,5-tetrafluorobenzene (the zero-dipole precursors) were presented in a previous study[21] and are included here for direct comparison. In the same previous study,[21] we also considered structures that had undergone significant structural rearrangement, the possibility of which is supported by the appearance of numerous fragment anions in the mass spectra. What was determined previously is that band **X** in the spectra was most consistent with an intact C_6 ring, with the original positioning of the −F substituents conserved. The computational results reported here reinforce the previous finding.

Figure 5 shows the computed relative energies of the difluorophenyl and difluorophenide species, again in the order of all-adjacent (group 1) to maximally spaced F atoms (group 3). The structures are shown on a relative energy scale, with the zero corresponding to the most stable difluorophenide anion determined computationally, 2,6-difluorophenide. The arrows connecting the anions and neutrals are labeled with the computed adiabatic EA. The relative energies of all species shown in Figure 5, along with the computed EAs and VDEs, are included in Table 1.

The 1,2-difluorobenzene precursor can form radicals with two different structures (group 1), one in which the radical center is adjacent to the fluorinated C center (2,3-difluorophenyl) and one that is meta with respect to a fluorinated C center (3,4-difluorophenyl), as shown in the top portion of Figure 5. The former is computed to be 0.06 eV higher in energy than the latter. The energy ordering is opposite in the anions, with the 2,3-fluorophenide being 0.41 eV lower in energy than the 3,4-fluorophenide structure. As a consequence, the difference in the computed EA for the two structures is 0.47 eV.

There are three possible structures in group 2 formed from 1,3-difluorobenzene, as shown in Figure 5. The least stable neutral radical structure of the three has a radical center between the two fluorinated C atoms (2,6-difluorophenyl) and corresponds to the most stable difluorophenide anion. The most stable radical is the one in which the radical center is furthest from the C−F sites (3,5-difluorophenide), which also corresponds to the least stable anion formed from this precursor structure. The three neutral radicals in this group are computed to be in a 0.25 eV window of energy, while the associated anions are in a 0.55 eV window of energy.

Finally, only one possible radical structure can be formed from the 1,4-difluorobenzene precursor, the computational results for which were previously published.[21] The neutral radical (2,5-difluorophenyl) and the associated anion lie within the windows of energy in which the neutrals and anions of the species formed from the 1,3-difluorobenzene precursor lie.

https://doi.org/10.1021/jacs.4c00556
J. Am. Chem. Soc. 2024, 146, 7063−7075

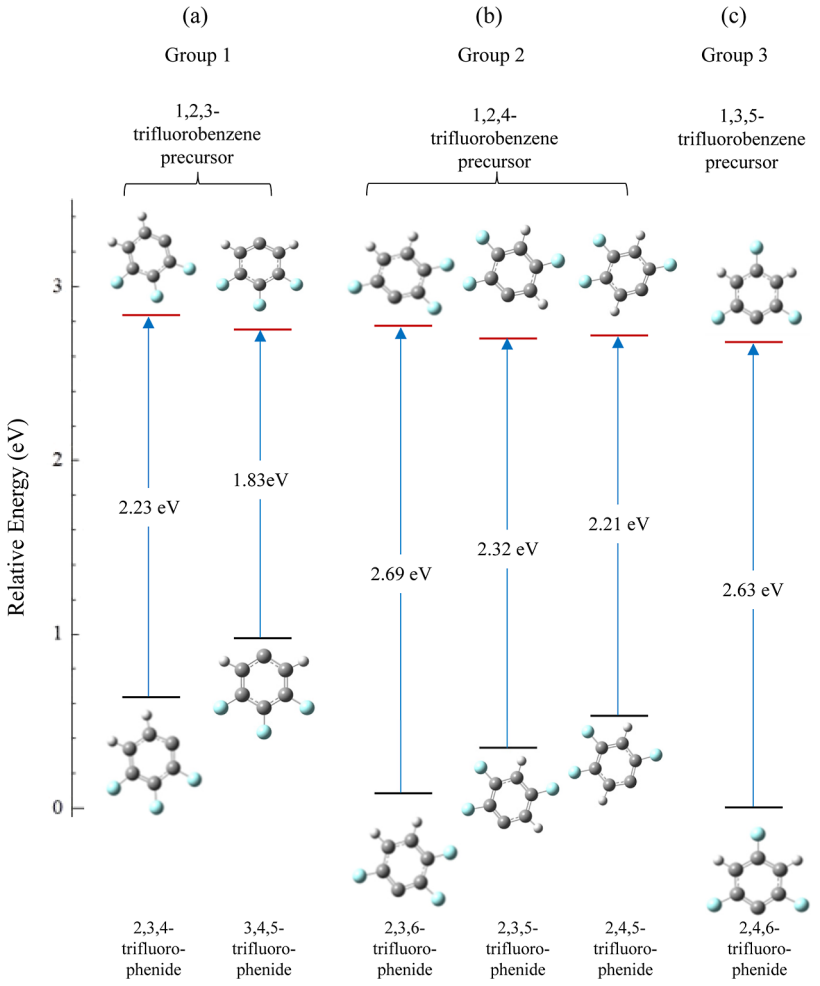

Figure 6. Computed relative energies of the neutral radicals and associated anions generated from homolytic C−H bond dissociation for (a) 1,2,3-trifluorobenzene (group 1), (b) 1,2,4-trifluorobenzene (group 2), and (c) 1,3,5-trifluorobenzene (group 3). The arrows connecting the anions to the associated neutral radicals are labeled with the computed adiabatic EAs, which are additionally indicated by arrows on the experimental spectra shown in Figure 2.

The relative energies of the anions in groups 1, 2, and 3 correlate with the computed proton affinities reported by Kato et al.:[66] the more stable anions have lower proton affinities; that is, the least amount of energy is required to deprotonate at the site that results in the most stable anion.

The computed adiabatic EAs of the neutral radicals associated with the lowest energy anions formed from the three different difluorobenzene precursors, 2,3-difluorophenide, 2,6-difluorophenide, and 2,5-difluorophenide, are indicated on the experimental spectra shown in Figure 1 as black arrows. The EAs of the radicals with higher-lying anion structures are shown with red arrows, with the dashed red arrow being associated with the highest-lying anion isomer for the three structures in group 2 (Figures 1b and 5]. The computed EAs for the radicals associated with the lower energy anions are modestly lower than but in very good agreement with the origins of band **X** in all three spectra. The other structures have computed EAs that are lower than the observed EA by approximately 0.5 eV.

The pattern of the most stable neutral radical having the least stable anion is almost entirely repeated in the trifluorophenyl series, as shown in Figure 6. All energies are relative to the most stable trifluorophenide anion identified computationally, 2,4,6-trifluorophenide. All six possible radical neutrals (two formed from 1,2,3-trifluorobenzene, three formed from 1,2,4-trifluorobenzene, and one from 1,3,5-trifluorobenzene) lie within a 0.2 eV window of energy, as summarized in Table 2. The relative energies of the anions span a wider 0.9 eV window of energy. The fact that the most stable radical structures correspond to less stable anions again leads to lower EAs for the most stable neutrals and higher EAs for the less stable neutrals. The computed adiabatic EAs are again indicated on the vertical arrows connecting the anions to their respective neutrals. These values along with the computed VDEs are included in Table 2, and the EAs are indicated on the experimental spectra in Figure 2. The black arrows again correspond to the lowest energy anionic structures, and solid red arrows correspond to the higher-lying anions, with the dashed red arrow in Figure 2b corresponding to the highest of three structural isomers in group 2. As with the difluorophenide series, the computed EAs associated with the most stable anions (least stable neutrals) are in good agreement with the experimental values, while those of the higher-lying anions are ca. 0.4 eV lower in energy than what is observed.

Figure 7 summarizes the relative energies of the three tetrafluorophenyl radicals and their respective anions. For each of the three precursor tetrafluorobenzene isomers, only one

https://doi.org/10.1021/jacs.4c00556
J. Am. Chem. Soc. 2024, 146, 7063−7075

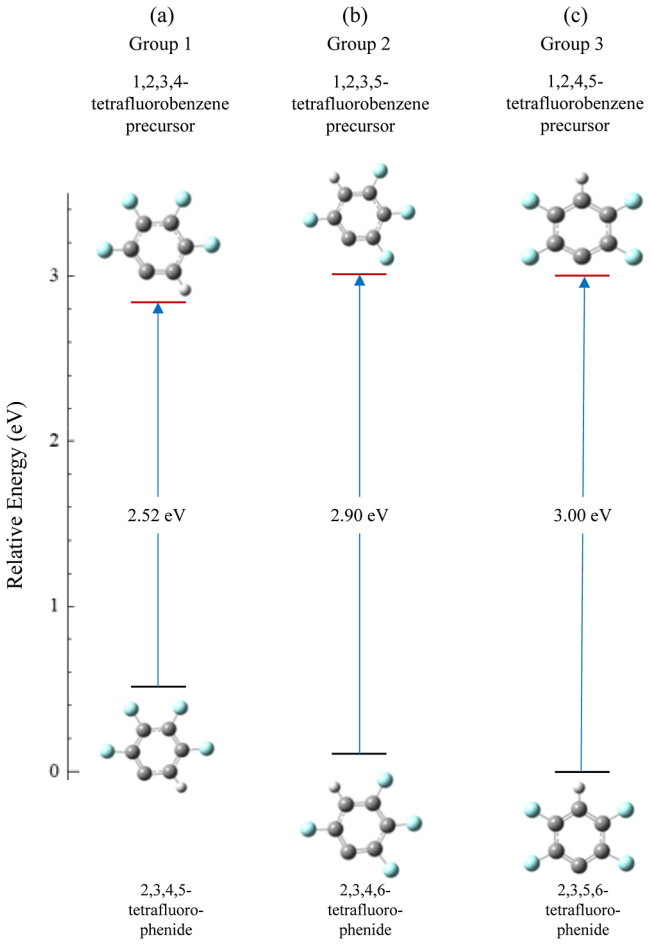

Figure 7. Computed relative energies of the neutral radicals and associated anions generated from homolytic C−H bond dissociation for (a) 1,2,3,4-tetrafluorobenzene (group 1), (b) 1,2,3,5-tetrafluorobenzene (group 2), and (c) 1,2,4,5-tetrafluorobenzene (group 3). The arrows connecting the anions to the associated neutral radicals are labeled with the computed adiabatic EAs, which are additionally indicated by arrows on the experimental spectra shown in Figure 3.

radical structure is possible. The three neutral radicals are computed to lie within a narrow 0.05 eV window of energy, while the anions span a 0.54 eV energy range. The computed adiabatic EAs are indicated on the arrows connecting the anions to the neutrals and are included in Table 3, along with the computed VDE values.

The computed EA values are also indicated in the experimental spectra shown in Figure 3. Note that the agreement between the computed EA of the sole isomer possible for each of the three precursor molecules (in order, as above, 1,2,3,4-tetrafluorobenzene, 1,2,3,5-tetrafluorobenzene, and 1,2,4,5-tetrafluorobenzene) is in good agreement with the observed spectra, and further reinforce the inferences above that the lowest energy anions of the less fluorinated phenides are the most abundant in the ion beam despite their associated radicals being less stable on the neutral surface. This result will be addressed in more detail in Section 4.

3.2.2. Molecular Structures. Details of the bond lengths and angles determined for anion ground states and the associated neutrals for all species are included in the Supporting Information. In brief, the structures of all anions and radical neutrals are predicted to be planar. The C−F bond lengths in the anions are predicted to be 0.05 to 0.06 Å longer than the neutral C−F bond lengths. The C−(C^-)−C bond angle in the anion is generally smaller than the C−($^\bullet$C)−C bond angle in the neutral by ca. 12°. As a result, the detachment transition bands are predicted to exhibit extended vibrational progressions and combination bands associated with C−F stretch modes, C_6 ring distortion modes, and in-plane −F and −H wagging modes. Neither the C−C nor the C−H bond lengths change significantly upon anion detachment.

PE spectral simulations based on the computed spectroscopic parameters for the four most active vibrational modes (EA, vibrational frequencies, and normal coordinate displacements) along with tables summarizing all anion and neutral vibrational frequencies and normal coordinate displacements are also included in the Supporting Information. While the simulated progressions are systematically less congested than the experimental spectra, which can be attributed to the limited number of modes included in the spectra (4 out of 27 total modes) and the limited appropriateness of the harmonic oscillator and parallel mode approximations, they are in qualitative agreement. The computed VDEs, and, more importantly, the difference between the computed VDE and EA (which reflects the predicted breadth of the vibrational manifold), are in better agreement with the observed spectra than the simulations.

3.2.3. Electronic Structures. Figures 8−10 show the frontier orbitals and their computed relative energies of the lowest energy anions formed for the three precursor regioisomers of difluorobenzene (Figure 8), trifluorobenzene (Figure 9), and tetrafluorobenzene (Figure 10). The in-plane orbital energies are indicated by red lines, and the out-of-plane π orbital energies are indicated by blue lines. The Supporting Information includes the orbital energies of the neutral radicals. The HOMO for each anion is the doubly occupied

Table 3. Summary of Computed Zero-Point Corrected Energies Relative to the 2,3,5,6-Tetrafluorophenide Anion (the Lowest Anion of All Tetrafluorophenides), Shown Graphically in Figure 7, in Addition to Adiabatic Detachment Energies, and Vertical Detachment Energies, for the Anionic Tetrafluorophenides and Corresponding Neutral Radicals[a]

molecule		electronic term	relative *E* (eV)	ADE/VDE (eV)	Exp ADE/VDE
1,2,3,4-tetrafluorobenzeneprecursor	2,3,4,5-tetrafluorophenyl radical	$^2A'$	3.05	2.52/2.84	2.63 ± 0.10/2.89 ± 0.05
	2,3,4,5-tetrafluorophenide	$^1A'$	0.54		
1,2,3,5-tetrafluorophenide precursor	2,3,4,6-tetrafluorophenyl radical	$^2A'$	3.01	2.90/3.24	2.97 ± 0.10/3.23 ± 0.05
	2,3,4,6-tetrafluorophenide	$^1A'$	0.11		
1,2,4,5-tetrafluorophenide precursor	2,3,5,6-tetrafluorophenyl radical	$^2A_1$	3.00	3.00/3.33	3.11 ± 0.10/3.41 ± 0.05
	2,3,5,6-tetrafluorophenide	$^1A_1$	0.00		

[a]Computed energies for 2,3,5,6-tetrafluorophenyl and 2,3,5,6-tetrafluorophenide were also reported in ref 21 and included here with permission from ref 21. Copyright 2023 American Chemical Society.

https://doi.org/10.1021/jacs.4c00556
J. Am. Chem. Soc. 2024, 146, 7063−7075

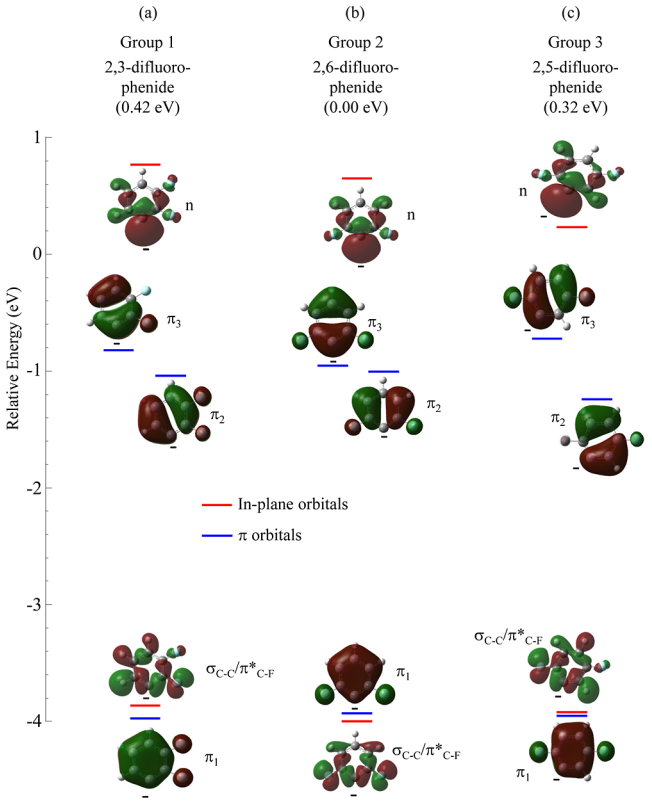

Figure 8. Depictions of valence orbitals (isovalue = 0.02) for the lowest energy structures computed for the difluorophenide anions in (a) group 1, (b) group 2, and (c) group 3. Relative energies of the three different species are included in parentheses.

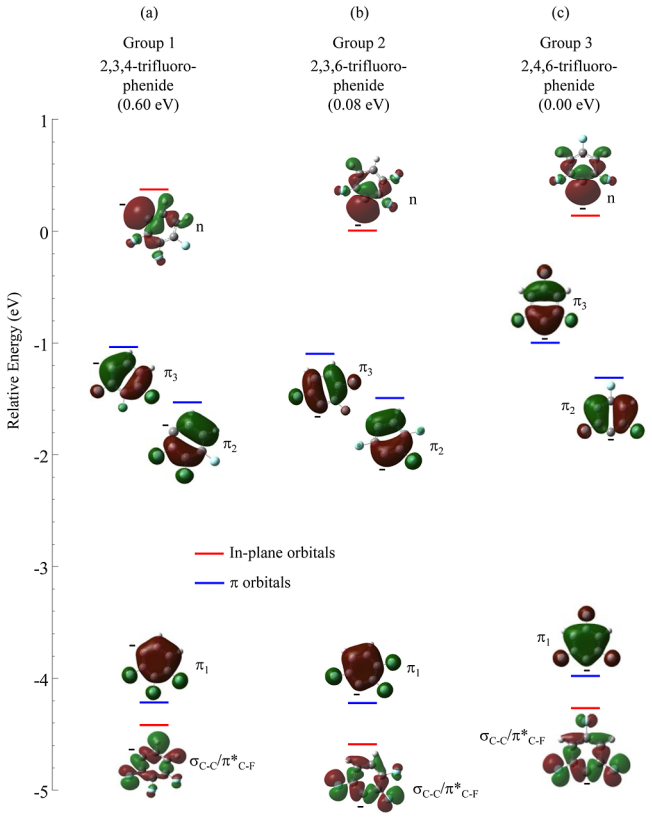

Figure 9. Depictions of valence orbitals (isovalue = 0.02) for the lowest energy structures computed for the trifluorophenide anions in (a) group 1, (b) group 2, and (c) group 3. Relative energies of the three different species are included in parentheses.

sp^2 nonbonding σ orbital (labeled "*n*") on the C-center coinciding with the radical center in the associated neutral. While the HOMOs for all nine species are modestly delocalized over the C_6 ring, the s−p hybridization is consistent with a PAD that is intermediate between isotropic and parallel, as was observed experimentally (Figure 4).[64,65]

We first consider the electronic structures of the difluorophene anions shown in Figure 8. All three have qualitatively similar orbital occupancies. Lying below the HOMO are the close-lying π orbitals, which are labeled π_2 and π_3 (which correlate to the π_2 and π_3 orbitals in the phenyl radical and the degenerate e_{1g} orbitals of benzene), which are C−C bonding and C−F antibonding. As described by Fuhrer et al.,[67] the π orbitals that are C−F bonding lie much lower in energy, and every F substitution is accompanied by an additional doubly occupied π orbital. Strictly speaking, the orbitals labeled π_2 and π_3 in Figure 8 are actually π_4 and π_5, but for the sake of a simple comparison between the di-, tri-, and tetrafluorophenide anions, we will adhere to labeling the frontier orbitals as shown. The π_1 orbital (C−F antibonding, fully C−C bonding) and an in-plane σ_{C-C}/π_{C-F}* orbital are close in energy.

From a survey of the three regioisomers of the difluorophenide anions, the relative energies of the frontier orbitals do not differ significantly. However, the most stable anion, 2,6-difluorophenide (Figure 8b), has the excess charge in the HOMO situated between two C−F centers, both of which are electron deficient (APT charges are tabulated in the Supporting Information). By virtue of the molecular symmetry (C_{2v}), the nodal plane of the π_2 orbital bisects the HOMO, which, as will be noted below, further stabilizes the excess charge but to a lesser extent than being located between two C−F centers.

The frontier orbitals of the most stable trifluorophenide anions shown in Figure 9 can be described in very similar terms, though with the additional −F substitution, the σ_{C-C}/π_{C-F}* orbitals are stabilized more relative to the π_1 orbital. The π_2 nodal plane cuts through the HOMO in both 2,3,4-trifluorophenide (Figure 9a) and 2,4,6-trifluorophenide (Figure 9c), but the former is much higher in energy than the latter, with the latter being stabilized because the excess charge in the HOMO is situated between two electron-deficient C−F centers. The excess charge in the 2,3,6-trifluorophenide anion (Figure 9b) is also between two C−F centers but is predicted to be 0.08 eV less stable than 2,4,6-trifluorophenide, which gives an estimate of the stabilizing effect of the π_2 nodal plane coinciding with the position of the excess charge.

The trends continue with the tetrafluorophenide anion frontier orbitals (Figure 10). The σ_{C-C}/π_{C-F}* orbitals are further stabilized more relative to the π_1 orbital. The stability bonus from the charge being situated between two F-substituted C-centers is ca. 0.5 eV, and the additional stability from the symmetry-allowed nodal plane bisecting the HOMO is ca. 0.1 eV.

The frontier orbitals of the neutral radicals are included in the Supporting Information. The isosurfaces of the orbitals appear very similar to those of the associated anions. However, the relative energy of the singly occupied molecular orbital (SOMO), which correlates to the HOMO of the anion, lies

https://doi.org/10.1021/jacs.4c00556
J. Am. Chem. Soc. 2024, 146, 7063−7075

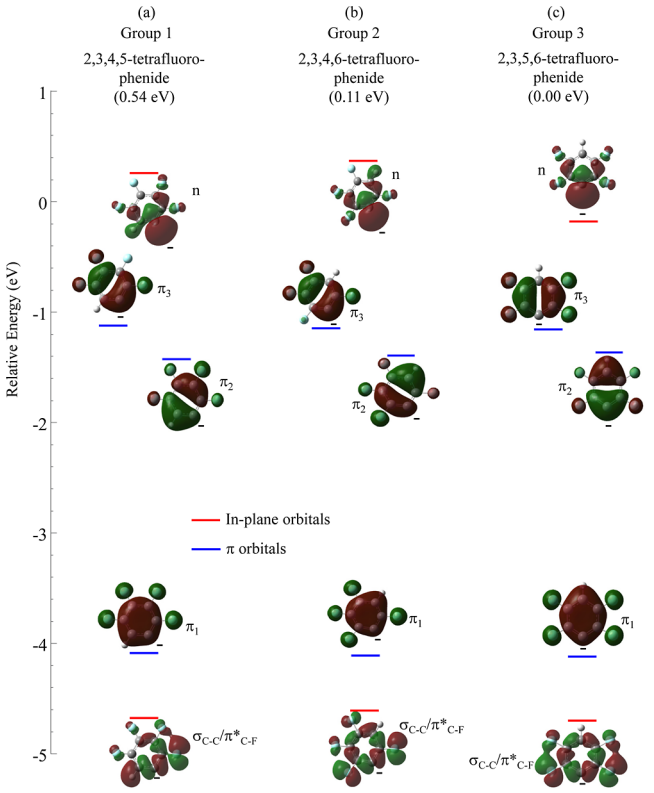

Figure 10. Depictions of valence orbitals (isovalue = 0.02) for the lowest energy structures computed for the tetrafluorophenide anions in (a) group 1, (b) group 2, and (c) group 3. Relative energies of the three different species are included in parentheses.

energetically below the π_2 and π_3 orbitals. This merely reflects that the unpaired electron is more strongly bound to the molecule than the electrons in the doubly occupied π_2 and π_3 orbitals.

4. DISCUSSION

The previous section reported and analyzed a range of experimental results on relative energies, electronic structures, and molecular structures, along with a comparison of the electronic and molecular structures of the radicals and their associated anions. Below, we attempt to connect the evidence above with the earlier assertion that the anions of fluorophenyl radicals could provide a tool for regioisomeric control.

4.1. Radical Structure versus EA. The relationship between the various radical structures and EA is intuitive within the following framework. Radical centers are electron deficient, whereas the same center upon anion formation is electron rich. The C−F centers (the fluorine-substituted C atoms) are also electron deficient, which is consistent with the lowest energy radical structures maximizing distance between C−F centers and •C centers, whereas the electron-rich −C center in the anion favors closer proximity to the C−F centers.

Figure 11 shows plots of the EA as a function of x. In Figure 11a, the computed EAs of the radicals correlated to the most stable anions are shown as open circles. There are a total of nine values associated with x = 2, 3, and 4 for groups 1 (blue), 2 (green), and 3 (red). In addition, for x = 2 and 3, groups 1 and 2 have additional possible structures, and the computed EA of the radical associated with the second lowest energy structures is shown as smaller squares (there is only one radical

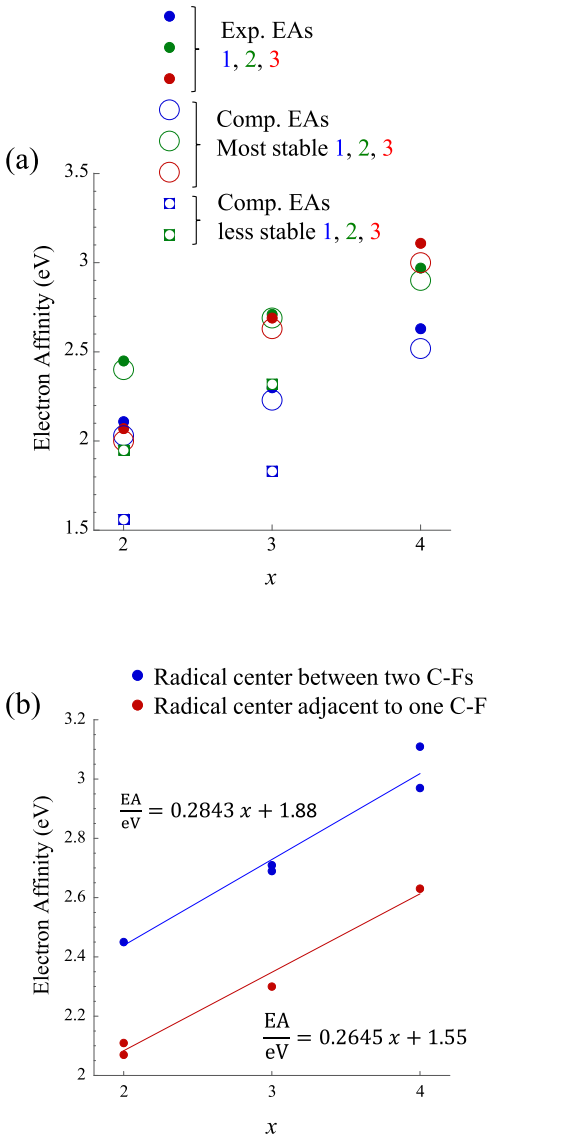

Figure 11. (a) Plot of the computed EAs of radicals associated with the most stable anions (large open circles), the second-most stable anions, where applicable (smaller square symbols) for $^{\bullet}C_6H_{5-x}F_x$ regioisomers in group 1 (blue), group 2 (green), and group 3 (red) as a function of x. Experimental values are included as small, solid circles. (b) Plot of experimental EAs for $^{\bullet}C_6H_{5-x}F_x$ regioisomers with the radical center situated between two F-substituted C-centers (blue) and those with the radical center adjacent to only one F-substituted C-center (red) as a function of x.

structure possible for the three tetrafluorophenyl regioisomers). The experimental EAs are shown as solid, small circles with the same color coding for groups 1, 2, and 3. This plot shows that the experimental values systematically track with the computed EAs for radicals associated with the lowest energy anions rather than the lowest energy radicals. The EAs computed for the more stable radicals (associated with the less stable anions) are systematically lower than the experimental values by approximately 0.5 eV.

A plot of the experimental EAs is shown in Figure 11b. For this plot, we assumed that the experimentally generated anions are consistent with the computed lowest energy structures and assigned red circles to structures in which the excess charge for the anion (radical center for the neutral) was adjacent to only

https://doi.org/10.1021/jacs.4c00556
J. Am. Chem. Soc. 2024, 146, 7063−7075

one C−F (group 1 for x = 2, 3, and 4; group 3 for x = 2) and blue circles for structures in which the excess charge for the anion (radical center for the neutral) is situated between two C−Fs. Separating the structures out in this matter results in two different trend lines, both with EAs increasing with x. From the plot, the EAs of radicals in which the radical center is between two C−Fs are over 0.3 eV higher than those with the radical center adjacent to one C−F.

The increase in experimental and computational EA with x, which experimentally is 0.27 ± 0.10 eV per x, has been shown in a previous study on a narrower set of fluorophenyl radicals[21] and correlates with the computed electron deficiency of the C_6 ring. The APT charges for the radicals (and anions) included in this study are in the Supporting Information; while the different regioisomers of each $^{\bullet}C_6H_{5-x}F_x$ have slightly different total APT charges on the C_6 ring for a given x, the difference is small compared to the variation in EA among the regioisomers (a plot of computed EA versus the sum of APT charge on the C centers is also included in the Supporting Information). The current study shows how structure impacts the EA on a scale comparable to that of the degree of fluorination!

4.2. Conservation of C−F Bonding during Ion Production and the Reliably Predictable Position of the Reactive Center on the Anion. The fact that the different radical structures associated with a single fluorobenzene precursor (see Figures 5a,b and 6a,b) are energetically within a 0.20 eV window reflects that for the neutral the C−H bond dissociation energies are not sensitive to the proximity to the C−F bond. While the mechanism(s) of the anion production in the source used in this study is not fully understood, the conditions under which the ions are formed are sufficiently energetic to produce a wide range of fragment anions (mass spectra are included in the Supporting Information). It is therefore possible that the higher-lying structures of the anions are being formed. For example, if the mechanism involves radical formation followed by electron attachment, it is entirely possible that, initially, 3,4-difluorophenide anions are being produced alongside 2,3-difluorophenide anions from the 1,2-difluorobenzene precursor (see Figure 5a). However, the clear tracking of the experimental EAs with the computed EAs of radicals that correlate to the lowest energy structures of anions with the original precursor C−F arrangement suggests that less stable anions can undergo a H-shift but not a F-shift. The length of time between ion production and detection is ca. 300 μs, which is well over the half-life of radical ring 1,2-H migration in radicals.[68] Once H-shifting results in the lowest energy structure of the anion, any subsequent shifting would involve barriers higher than those leading to the most stable structure.

Of course, by symmetry, five of the nine anions included in this study have only one possible position of the excess charge, so the reactive centers of the anion and the associated neutral radical are identical. For the remaining four groups (groups 1 and 2 of the di- and trifluorophenides), the reactive center of the anion is both predictable and different from the most stable associate neutral radical.

5. CONCLUSIONS

The PE spectra of the $C_6H_{5-x}F_x^-$ ($2 \le x \le 4$) fluorophenide anions generated from the three regioisomers of $C_6H_{6-x}F_x$ ($2 \le x \le 4$) are presented and compared to DFT calculations on the anions and associated neutral radicals. For the sake of clarity, we categorized the regioisomers as group 1 (all x F atoms on adjacent C atoms), group 2 (x − 1 F atoms on adjacent C atoms), and group 3 (F atoms maximally separated). The key findings are as follows:

1 Within group 1 and group 2 of di- and trifluorophenyl radicals, the most stable anions do not correspond to the most stable neutral radical. Therefore, the reactive center on the anion is different from the radical's reactive center, offering a charge-state based structural handle on syntheses involving fluorophenyl addition reactions.
2 The anions formed from the precursor fluorobenzene regioisomers appear to conserve the F-arrangements of the precursor. There is no evidence that rearrangement of F atoms on the C_6 ring is occurring in the ion source.
3 From the computational results, the multiple radicals formed for any given x lie in a narrow window of energy compared to the anions. The energy of the anions is more sensitive to the position of the excess charge relative to the F substituents.
4 As determined both experimentally and computationally, the EA of the neutral radicals in this study depends linearly on x, but the EAs of radicals in which the radical center is situated between two F-substituted C-center is ca. 0.35 eV higher than radicals in which the radical center is adjacent to one F-substituted C-center.

■ ASSOCIATED CONTENT

Supporting Information

The Supporting Information is available free of charge at https://pubs.acs.org/doi/10.1021/jacs.4c00556.

Number of laser shots over which the 18 spectra were accumulated, raw and reconstructed PE images, the mass spectra of anions generated from parent fluorobenzene seeded in He via the photoemission source, isosurfaces of the frontier orbitals of the anions and neutrals, APT charges, and computed bond lengths and angles of the possible regioisomer structures of $C_6H_{5-x}F_x^-$ and $^{\bullet}C_6H_{5-x}F_x$ (x = 2−4), computed vibrational frequencies, normal coordinate displacements calculated for the detachment transitions, and spectral simulations (PDF)

■ AUTHOR INFORMATION

Corresponding Author

Caroline Chick Jarrold − *Department of Chemistry, Indiana University, Bloomington, Indiana 47405, United States;* orcid.org/0000-0001-9725-4581; Email: cjarrold@indiana.edu

Authors

Kristen Rose McGinnis − *Department of Chemistry, Indiana University, Bloomington, Indiana 47405, United States*

Conor J. McGee − *Department of Chemistry, Indiana University, Bloomington, Indiana 47405, United States*

Complete contact information is available at: https://pubs.acs.org/10.1021/jacs.4c00556

Notes

The authors declare no competing financial interest.

■ ACKNOWLEDGMENTS

This material is based upon work supported by the National Science Foundation under grant no. 2053889.

REFERENCES

(1) Porter, G.; Ward, B. The Electronic Spectra of Phenyl Radicals. *Proc. R. Soc. London* **1965**, *287*, 457−470.
(2) Friderichsen, A. V.; Radziszewski, J. G.; Nimlos, M. R.; Winter, P. R.; Dayton, D. C.; David, D. E.; Ellison, G. B. The Infrared Spectrum of the Matrix-Isolated Phenyl Radical. *J. Am. Chem. Soc.* **2001**, *123*, 1977−1988.
(3) Chang, C.-H.; Nesbitt, D. J. High Resolution Spectroscopy of Jet Cooled Phenyl Radical: The v_1 and v_2 a_1 Symmetry C−H Stretching Modes. *J. Chem. Phys.* **2016**, *145*, 044304.
(4) Sharp, E. N.; Roberts, M. A.; Nesbitt, D. J. Rotationally Resolved Infrared Spectroscopy of a Jet-Cooled Phenyl Radical in the Gas Phase. *Phys. Chem. Chem. Phys.* **2008**, *10*, 6592−6596.
(5) Freel, K.; Park, J.; Lin, M. C.; Heaven, M. C. Cavity Rign-Down Spectroscopy of the Phenyl Radical in a Pulsed Discharge Supersonic Jet Expansion. *Chem. Phys. Lett.* **2011**, *507*, 216−2020.
(6) Radziszewski, J. G. Electronic Absorption Spectrum of Phenyl Radical. *Chem. Phys. Lett.* **1999**, *301*, 565−570.
(7) Cole-Filipiak, N. C.; Shapero, M.; Negru, B.; Neumark, D. M. Revisiting the Photodissociation Dynamics of the Phenyl Radical. *J. Chem. Phys.* **2014**, *141*, 104307.
(8) Gunion, R. F.; Gilles, M. K.; Polak, M. L.; Lineberger, W. C. Ultraviolet Photoelectron Spectroscopy of the Phenide, Benzyl and Phenoxide anions, with ab initio Calculations. *Int. J. Mass Spectrom. Ion Processes* **1992**, *117*, 601−620.
(9) Miller, J. A.; Pilling, M. J.; Troe, J. Unravelling Combustion Mechanisms through a Quantitative Understanding of Elementary Reactions. *Proc. Combust. Inst.* **2005**, *30*, 43−88.
(10) Richter, H.; Howard, J. B. Formation of Polycyclic Aromatic Hydrocarbons and their Growth to Soot- A Review of Chemical Reaction Pathways. *Prog. Energy Combust. Sci.* **2000**, *26*, 565−608.
(11) Guelin, M.; Cernicharo, J. Organic Molecules in Interstellar Space: Latest Advances. *Astronaut. Space Sci.* **2022**, *9*, 787567.
(12) McMahon, R. J.; McCarthy, M. C.; Gottlieb, C. A.; Dudek, J. B.; Stanton, J. F.; Thaddeus, P. The Radio Spectrum of the Phenyl Radical. *Astrophys. J.* **2003**, *590*, L61−L64.
(13) McGuire, B. A.; Loomis, R. A.; Burkhardt, A. M.; Lee, K. L. K.; Shingledecker, C. N.; Charnley, S. B.; Cooke, I. R.; Cordiner, M. A.; Herbst, E.; Kalenskii, S.; et al. Detection of Two Interstellar Polycyclic Aromatic Hydrocarbons via Spectral Matched Filtering. *Science* **2021**, *371*, 1265−1269.
(14) Wall, L. A.; Pummer, W. J.; Fearn, J. E.; Antonucci, J. M. Reactions of Polyfluorobenzenes With Nucleophilic Reagents. *J. Res. Natl. Bur. Stand., Sect. A* **1963**, *67A*, 481−497.
(15) Fuhrer, T. J.; Houck, M.; Iacono, S. T. Fluoromaticity: The Molecular Orbital Contributions of Fluorine Substituents to the π-Systems of Aromatic Rings. *ACS Omega* **2021**, *6*, 32607−32617.
(16) Ege, S. *Organic Chemistry*; D.C. Heath and Company: Lexington, Mass, 1984.
(17) Bond Dissociation Energies. *CRC Handbook of Chemistry and Physics*, 104th ed.; (Internet Version 2023); Rumble, J. R., Ed.; CRC Press/Taylor & Francis: Boca Raton, FL, 2023.
(18) Dobulis, M. A.; Thompson, M. C.; Sommerfeld, T.; Jarrold, C. C. Temporary anion states of fluorine substituted benzenes probed by charge transfer in $O_2^-{\cdot}C_6H_{6-x}F_x$ (x = 0−5) ion−molecule complexes. *J. Chem. Phys.* **2020**, *152*, 204309.
(19) McGee, C. J.; McGinnis, K. R.; Jarrold, C. C. Anion Photoelectron Imaging Spectroscopy of $C_6HF_5^-$, $C_6F_6^-$, and the Absence of $C_6H_2F_4^-$. *J. Phys. Chem. A* **2023**, *127*, 8556−8565.
(20) Davis, J. U.; Chick Jarrold, C.; Sommerfeld, T. Charge Distribution in Oxygen-Fluorobenzene Complex Anions $[O_2{\cdot}C_6H_{6-n}F_n]^-$ (n = 0 − 6). *Chem. Phys.* **2023**, *574*, 112023.
(21) McGee, C. J.; McGinnis, K. R.; Jarrold, C. C. Trend in the Electron Affinities of Fluorophenyl Radicals, $\cdot C_6H_{(5-x)}F_x$. *J. Phys. Chem. A* **2023**, *127*, 7264−7273.
(22) Rankovic, M.; Nag, P.; Anstöter, C. S.; Mensa-Bonsu, G.; Kumar T P, R.; Verlet, J. R. R.; Fedor, J. Resonances in Nitrobenzene Probed by the Electron Attachment to Neutral and by the Photodetachment from Anion. *J. Chem. Phys.* **2022**, *157*, 064302.
(23) Demir, Y.; Türkeş, C.; Küfrevioğlu, Ö. İ.; Beydemir, Ş. Molecular Docking Studies and the Effect of Fluorophenylthiourea Derivatives on Glutathione-Dependent Enzymes. *Chem. Biodivers.* **2023**, *20*, No. e202200656.
(24) Cairi, M.; Gerig, J. T. Fluorine recognition at the active site of [N-(4-fluorophenyl)-N-phenylcarbamoyl]-.alpha.-chymotrypsin. *J. Am. Chem. Soc.* **1984**, *106*, 3640−3643.
(25) Shinya, S.; Kawai, K.; Kobayashi, N.; Karuo, Y.; Tarui, A.; Sato, K.; Otsuka, M.; Omote, M. Fluorophenylalkyl-Substituted Cyanoguanidine Derivatives as Bacteria-Selective MATE Transporter Inhibitors for the Treatment of Antibiotic-Resistant Infections. *Bioorg. Med. Chem.* **2022**, *74*, 117042.
(26) Zhao, W.; Yang, Y.; Zhang, Y.-X.; Zhou, C.; Li, H.-M.; Tang, Y.-L.; Liang, X.-H.; Chen, T.; Tang, Y.-J. Fluoride-Containing Podophyllum Derivatives Exhibit Antitumor Activities through Enhancing Mitochondrial Apoptosis Pathway by Increasing the Expression of Caspase-9 in HeLa Cells. *Sci. Rep.* **2015**, *5*, 17175.
(27) Kim, C.-Y.; Chang, J. S.; Doyon, J. B.; Baird, T. T.; Fierke, C. A.; Jain, A.; Christianson, D. W. Contribution of Fluorine to Protein−Ligand Affinity in the Binding of Fluoroaromatic Inhibitors to Carbonic Anhydrase II. *J. Am. Chem. Soc.* **2000**, *122*, 12125−12134.
(28) Anisuzzaman, S.; Geraskin, I. M.; Ilgu, M.; Bendickson, L.; Kraus, G. A.; Nilsen-Hamilton, M. Ligands with Polyfluorophenyl Moieties Promote a Local Structural Rearrangement in the Spinach2 and Broccoli Aptamers that Increases Ligand Affinities. *RNA* **2022**, *28*, 865−877.
(29) Donabauer, K.; König, B. Strategies for the Photocatalytic Generation of Carbanion Equivalents for Reductant-Free C−C Bond Formations. *Acc. Chem. Res.* **2021**, *54*, 242−252.
(30) Wenthold, P. G.; Squires, R. R.; Lineberger, W. C. Ultraviolet Photoelectron Spectroscopy of the *o*-*m*-and *p*-Benzyne Negative Ions. Electron Affinities and Singlet-Triplet Splittings for *o*-*m*-and *p*-Benzyne. *J. Am. Chem. Soc.* **1998**, *120*, 5279−5290.
(31) Gibbard, J. A.; Continetti, R. E. Photoelectron Photofragment Coincidence Spectroscopy of Carboxylates. *RSC Adv.* **2021**, *11*, 34250−34261.
(32) Gibbard, J. A.; Castracane, E.; Shin, A. J.; Continetti, R. E. Dissociative Photodetachment Dynamics of the Oxalate Monoanion. *Phys. Chem. Chem. Phys.* **2020**, *22*, 1427−1436.
(33) Lunny, K. G.; Benitez, Y.; Albeck, Y.; Strasser, D.; Stanton, J. F.; Continetti, R. E. Spectroscopy of Ethylenedione and Ethynediolide: A Reinvestigation. *Angew. Chem., Int. Ed.* **2018**, *57*, 5394−5397.
(34) Benitez, Y.; Nguyen, T. L.; Parsons, A. J.; Stanton, J. F.; Continetti, R. E. Probing the Exit Channel of the OH + CH_3OH → H_2O + CH_3O Reaction by Photodetachment of $CH_3O^-(H_2O)$. *J. Phys. Chem. Lett.* **2022**, *13*, 142−148.
(35) Schwartz, R. L.; Davico, G. E.; Ramond, T. M.; Lineberger, W. C. Singlet-Triplet Splittings in CX_2 (X = F, Cl Br, I) Dihalocarbenes via Negative Ion Photoelectron Spectroscopy. *J. Phys. Chem. A* **1999**, *103*, 8213−8221.
(36) Bouwman, J.; Hrodmarsson, H. R.; Ellison, G. B.; Bodi, A.; Hemberger, P. Five Birds with One Stone: Photoelectron Photoion Coincidence Unveils Rich Phthalide Pyrolysis Chemistry. *J. Phys. Chem. A* **2021**, *125*, 1738−1746.
(37) Ru, B.; Sanov, A. Photoelectron Spectra of Hot Polyatomic Ions: A Statistical Treatment of Phenide. *J. Phys. Chem. A* **2022**, *126*, 9423−9439.
(38) Culberson, L. M.; Blackstone, C. C.; Wallace, A. A.; Sanov, A. Aromatic Stabilization and Hybridization Trends in Photoelectron Imaging of Heterocyclic Radicals and Anions. *J. Phys. Chem. A* **2015**, *119*, 9770−9777.
(39) Wallace, A. A.; Dauletyarov, Y.; Sanov, A. Diradical Interactions in Ring-Open Isoxazole. *J. Phys. Chem. A* **2021**, *125*, 317−326.
(40) Laws, B. A.; Levey, Z. D.; Sanov, A.; Stanton, J. F.; Schmidt, T. W.; Gibson, S. T. Velocity Map Imaging Spectroscopy of C_2H^- and C_2D^-: A Benchmark Study of Vibronic Coupling Interactions. *J. Chem. Phys.* **2022**, *157*, 044305.
(41) Dixon, A. R.; Khuseynov, D.; Sanov, A. Heterogeneously Substituted Radicals and Carbenes: Photoelectron Imaging of the

https://doi.org/10.1021/jacs.4c00556
J. Am. Chem. Soc. 2024, 146, 7063−7075

FC(H)CN$^-$ and FCCN$^-$ Anions. *J. Phys. Chem. A* **2014**, *118*, 8533−8541.
(42) Anstöter, C. S.; Rogers, J. P.; Verlet, J. R. Spectroscopic Determination of an Anion−π Bond Strength. *J. Am. Chem. Soc.* **2019**, *141*, 6132−6135.
(43) Hossain, E.; Deng, S. M.; Gozem, S.; Krylov, A. I.; Wang, X. B.; Wenthold, P. G. Photoelectron Spectroscopy Study of Quinonimides. *J. Am. Chem. Soc.* **2017**, *139*, 11138−11148.
(44) Lau, J. A.; DeWitt, M.; Boyer, M. A.; Babin, M. C.; Solomis, T.; Grellmann, M.; Asmis, K. R.; McCoy, A. B.; Neumark, D. M. High-Resolution Photoelectron Spectroscopy of Vibrationally Excited Vinoxide Anions. *J. Phys. Chem. A* **2023**, *127*, 3133−3147.
(45) DeWitt, M.; Babin, M. C.; Lau, J. A.; Solomis, T.; Neumark, D. M. High Resolution Photoelectron Spectroscopy of the Acetyl Anion. *J. Phys. Chem. A* **2022**, *126*, 7962−7970.
(46) DeVine, J. A.; Babin, M. C.; Blackford, K.; Neumark, D. M. High-Resolution Photoelectron Spectroscopy of the Pyridinide Isomers. *J. Chem. Phys.* **2019**, *151*, 064302.
(47) Harrison, A. W.; Ryazanov, M.; Sullivan, E. N.; Neumark, D. M. Photodissociation Dynamics of the Methyl Perthiyl Radical at 248 and 193 nm using Fast-Beam Photofragment Translational Spectroscopy. *J. Chem. Phys.* **2016**, *145*, 024305.
(48) Neumark, D. M. Spectroscopy of Radicals, Clusters, and Transition States Using Slow Electron Velocity Map Imaging of Cryogenically Cooled Anions. *J. Phys. Chem. A* **2023**, *127*, 4207−4223.
(49) Stokes, S. T.; Bartmess, J. E.; Buonaugurio, A.; Wang, Y.; Eustis, S. N.; Bowen, K. H. Anion Photoelectron Spectroscopy of the Linear $C_nH_{2n+1}O^-$ (n = 1−9) Alkoxides. *Chem. Phys. Lett.* **2019**, *732*, 136638.
(50) Patros, K. M.; Mann, J. E.; Dobulis, M. A.; Thompson, M. C.; Jarrold, C. C. Probing Alkenoxy Radical Electronic Structure using Anion PEI Spectroscopy. *J. Chem. Phys.* **2019**, *150*, 034302.
(51) Mann, J. E.; Troyer, M. E.; Jarrold, C. C. Photoelectron Imaging and Photodissociation of Ozonide in $O_3^-\cdot(O_2)_n$ (n = 1 − 4). *J. Chem. Phys.* **2015**, *142*, 124305.
(52) Williams, B. A.; Siedle, A. R.; Jarrold, C. C. Identification of Stable Perfluorocarbons Formed by Hyperthermal Decomposition of Graphite Fluoride Using Anion Photoelectron Spectroscopy. *J. Phys. Chem. C* **2022**, *126*, 9965−9978.
(53) Eppink, A. T. J. B.; Parker, D. H. Velocity Map Imaging of Ions and Electrons using Electrostatic Lenses: Application in Photoelectron and Photofragment Ion Imaging of Molecular Oxygen. *Rev. Sci. Instrum.* **1997**, *68*, 3477−3484.
(54) Chandler, D. W.; Houston, P. L. Two-Dimensional Imaging of State-Selected Photodissociation Products Detected by Multiphoton Ionization. *J. Chem. Phys.* **1987**, *87*, 1445−1447.
(55) Doyle, M. B.; Abeysekera, C.; Suits, A. G. NuAcq 0.9: Native Megapixel Ion Imaging with Centroiding to 4 Mpix Using Inexpensive USB-2 Cameras. http://faculty.missouri.edu/suitsa/NuAqc.html (accessed Feb 4, 2020).
(56) Dribinski, V.; Ossadtchi, A.; Mandelshtam, V. A.; Reisler, H. Reconstruction of Abel-Transformable Images: The Gaussian Basis-Set Expansion Abel Transform Method. *Rev. Sci. Instrum.* **2002**, *73*, 2634−2642.
(57) Ervin, K. M.; Anusiewicz, I.; Skurski, P.; Simons, J.; Lineberger, W. C. The Only Stable State of O_2^- is the X $^2\Pi_g$ Ground State and it (Still!) Has an Adiabatic Electron Detachment Energy of 0.45 eV. *J. Phys. Chem. A* **2003**, *107*, 8521−8529.
(58) Hajgató, B.; Deleuze, M. S.; Tozer, D. J.; De Proft, F. A Benchmark Theoretical Study of the Electron Affinities of Benzene and Linear Acenes. *J. Chem. Phys.* **2008**, *129*, 084308.
(59) Firsch, M. J.; Trucks, G. W.; Schlegel, H. B.; Scuseria, G. E.; Robb, M. A.; Cheeseman, J. R.; Scalmani, G.; Barone, V.; Mennucci, B.; Petersson, G. A.; et al. *Gaussian 16*; Gaussian Inc.: Wallingford, CT, USA, 2016.
(60) Schaugaard, R. N.; Topolski, J. E.; Ray, M.; Raghavachari, K.; Jarrold, C. C. Insight into Ethylene Interactions with Molybdenum Suboxide Cluster Anions from Photoelectron Spectra of Chemifragments. *J. Chem. Phys.* **2018**, *148*, 054308.
(61) Zare, R. N. Photoejection Dynamics [1]. *Mol. Photochem.* **1972**, *4*, 1−37.
(62) Cooper, J.; Zare, R. N. Angular Distribution of Photoelectrons. *J. Chem. Phys.* **1968**, *48*, 942−943.
(63) Cooper, J.; Zare, R. N. Erratum: Angular Distribution of Photoelectrons. *J. Chem. Phys.* **1968**, *49*, 4252.
(64) Khuseynov, D.; Blackstone, C. C.; Culberson, L. M.; Sanov, A. Photoelectron Angular Distributions for States of any Mixed Character: An Experiment-Friendly Model for Atomic, Molecular, and Cluster Anions. *J. Chem. Phys.* **2014**, *141*, 124312.
(65) Sanov, A. Laboratory-Frame Photoelectron Angular Distributions in Anion Photodetachment: Insight into Electronic Structure and Intermolecular Interactions. *Annu. Rev. Phys. Chem.* **2014**, *65*, 341−363.
(66) Kato, S.; DePuy, C. H.; Gronert, S.; Bierbaum, V. M. Gas Phase Hydrogen/Deuterium Exchange Reactions of Fluorophenyl Anions. *J. Am. Soc. Mass Spectrom.* **1999**, *10*, 840−847.
(67) Fuhrer, T. J.; Houck, M.; Iacono, S. T.; Iacono; Scott, T. Fluoromaticity: The Molecular Orbital Contributions of Fluorine Substituents to the π-Systems of Aromatic Rings. *ACS Omega* **2021**, *6*, 32607−32617.
(68) Pezacki, J. P.; Couture, P.; Dunn, J. A.; Warkentin, J.; Wood, P. D.; Lusztyk, J.; Ford, F.; Platz, M. S. Rate Constants for 1,2-Hydrogen Migration in Cyclohexylidene and in Substituted Cyclohexylidenes. *J. Org. Chem.* **1999**, *64*, 4456−4464.

https://doi.org/10.1021/jacs.4c00556
J. Am. Chem. Soc. 2024, 146, 7063−7075